Proceedings of the International School and Conference on Photonics, PHOTONICA09

# Thermodynamic Temperature and Density of Ar(I) for $4S'[1/2]0$ State in a Facing Target Sputtering System

Y. Yasuda*, N. Nishimiya, Y. Hoshi and M. Suzuki

Department of Electronics and Information Technology

Tokyo Polytechnic University, Kanagawa, Japan

The $4S'[1/2]0 \rightarrow 4P'[3/2]1$ transition of Ar(I) in a facing target sputtering chamber is measured using a Ti:sapphire ring laser at several operating conditions. Doppler width and line intensity are determined by analysis using the Voigt function. The thermodynamic temperature determined from the Doppler width increases linearly with discharge current and gas pressure. The population density from the line intensity is reduced to the reference temperature obtained by interpolating the discharge current to zero. The empirical relationship to describe population density at a discharge current and a gas pressure is discussed.

PACS numbers: 32.30.–r, 42.62.Fi, 52.70.–m

## 1. Introduction

Recently, there has been considerable interest in facing target sputtering (FTS), which enables high deposition rates without substrate heating, and is therefore useful for deposition on organic thin films. Organic light-emitting devices (OLEDs) have attracted much attention as promising next-generation flat-panel displays. Uchida et al. fabricated transparent flexible OLEDs on a plastic film substrate [1]. Hoshi et al. reported that bombardment of the substrate by high-energy particles and secondary electrons can be suppressed completely by means of FTS methods [2, 3].

Although the thermodynamic temperature of the gas in a sputtering chamber is important to the success of sputter deposition on films, it is difficult to measure the gas temperature. A number of researchers attempted to perform plasma diagnostics using a spectrometer, but to the best of our knowledge, the temperature and density of the gas in an FTS system have not been investigated in detail. In general, particle temperature and density are determined by measuring linewidth and intensity [4, 5]. However, the absorption or emission lines in a sputtering chamber are deformed by the Zeeman effect and the limit of the resolving power of the spectrometer, which make it difficult to determine the temperature and density of the particles.

Absorption spectroscopy using a tunable laser is useful from the viewpoint of resolving power and polarizing characteristics. FTS offers several advantages over conventional magnetron sputtering, because the magnetic field is homogeneous and the plasma region is confined between the targets. Argon is commonly used as the sputtering gas. Many electronic transitions in the near infrared wavelength region are reported with physical constants [6].

We selected, as a first approach, the Ar(I)$4S'[1/2]0 \rightarrow 4P'[3/2]1$ transition (794.8 nm). It has only one Zeeman component, $M_J = 0 \rightarrow 0$, when the polarization axis of the laser beam is parallel to the field axis. A Voigt line profile was used for the analysis; the Doppler width and line intensity were selected as fitting parameters. The density of the metastable state $4S'[1/2]0$ was calculated from the line intensity and reduced to that at the reference temperature obtained by interpolating the discharge current to zero. This procedure is useful for eliminating the temperature variation that accompanies changes in discharge current and sputtering gas pressure. The reduced densities thus obtained offer an important physical quantity for plasma dynamics.

## 2. Experimental setup

The FTS chamber is shown in Fig. 1. Two sputtering titanium targets are arranged facing each other. A static field of about 500 G (measured by Gauss meter) is generated by NbFeB magnets inside the targets.

The diameter of the targets that are cooled by water is 50 mm. The gap between them is 80 mm. The gas pressure of Ar in the chamber is maintained in the range 2.0–20 Pa; the background pressure is below $1.3 \times 10^{-4}$ Pa. Glow discharge is produced by a DC source at a current in the range 1–400 mA. The diameter of the plasma region confined by the magnetic field is around 80 mm. A White-type optical pass is arranged to obtain a longer absorption pass length of 320 mm. The silica windows are tilted with respect to the laser beam at a Brewster angle to reduce reflection loss.

* corresponding author; e-mail: yyasuda@seit.t-kougei.ac.jp

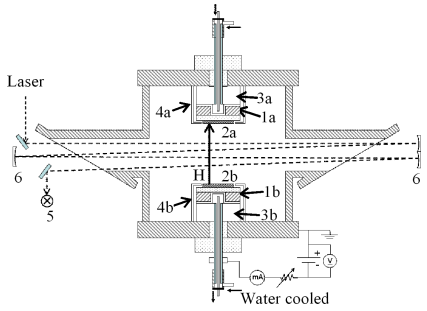


Fig. 1. Schematic drawing of the FTS and laser beam configuration. 1 — NdFeB magnet; 2 — titanium target; 3 — yoke; 4 — shield cylinder; 5 — photodetector; 6 — concave mirror.

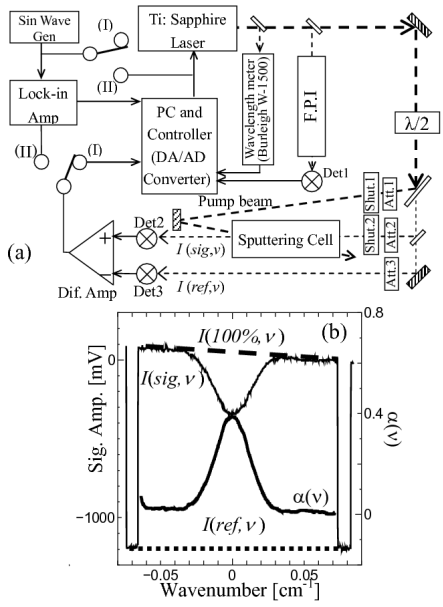


Fig. 2. Laser spectrometer used for the experiment. (a) Experimental optical pass arrangement and signal processor. (b) Absorption signal of the $4S'[1/2]0 \rightarrow 4P'[3/2]1$ transition at 1.3 Pa and fixed 200 mA discharge current.

The optical and electrical system is shown in Fig. 2a. A CW Ti:sapphire ring laser (Coherent 899-21) pumped by a YAG laser (Coherent Verdi-V8) is used as a radiation source. The laser wavelength is measured using a wavelength meter (Burleigh WA-1500) and the fine frequency is tuned using a triangular wave generated from a D/A converter. Spectra are recorded for the fringe signals of 0.010 $\mathrm{cm}^{-1}$ spacing generated by a confocal Fabry–Perot interferometer of 250 mm length with polarization parallel to the magnetic field. The laser beam is divided into three beams using beam splitters: the first (thick dotted line) is for pumping, the second for probing the spectral line, and the third for reference to calibrate power change in the tuning range.

## 3. Results and discussion

The absorption line profile was taken as the difference between $I(sig, \nu)$ and $I(ref, \nu)$ detected by detectors 2 and 3, respectively. The magnetic field was obtained from the saturated absorption lines for $4S[3/2]1 \rightarrow 4P[3/2]1$ (810.4 nm) and $4S'[1/2]0 \rightarrow 4P'[3/2]1$ (794.8 nm). Signals were detected by a wavelength modulation method at the SW position (II). The former line splits into the Zeeman doublet by the selection rule $M_J = \pm 1 \rightarrow \pm 1$; the latter line showed only one Zeeman component, $M_J = 0 \rightarrow 0$. Splittings for transitions $4S[3/2]1 \rightarrow 4P[5/2]2$, $4S[3/2]2 \rightarrow 4P[5/2]2$, and $4S[3/2]1 \rightarrow 4P[5/2]3$ were also detected. We confirmed that the magnetic field was parallel to the polarization direction. The effective magnetic field was calculated to be $445 \pm 5$ G from the line splittings and the g-factors [6]. It is clear that the transition $4S'[1/2]0 \rightarrow 4P'[3/2]1$ is suitable for analysis of line profile and intensity.

Changing the SW position to (I) and closing shutter 1 enables us to measure the Doppler-limited spectra. Figure 2b shows the differential output between the signals of detectors 2 and 3. Trace for $I(sig, \nu)$ shows the detected signal in wavenumber scale. Dips at both sides are obtained by closing shutter 2. The dotted line at the bottom is the baseline; the broken line at the top for $I(100\%, \nu)$ is the absorptionless power level. The relation between transmittance $T(\nu)$ and absorbance $\alpha(\nu)$ is given by

$$T(\nu) = \frac{I(sig, \nu) - I(ref, \nu)}{I(100\%, \nu) - I(ref, \nu)} = \exp[-\alpha(\nu)]. \qquad (1)$$

To investigate the saturation effect on line intensity and linewidth, we attenuated the input power by varying attenuator 2 from 5 to 10 $\mu$W. The line profile is commonly given by a Voigt function [7]

$$\alpha(\nu) = S \int_{\infty}^{\infty} G(0, \nu_0) \cdot L(\nu', \nu)\, \mathrm{d}\nu', \qquad (2)$$

where $G(\nu', \nu_0)$ is the normalized Gaussian function, $\nu_0$ is the line center, and $L(\nu', \nu)$ is the normalized Lorentzian, and $S$ is the line intensity (in $\mathrm{cm}^{-1}$) for cell length $L$. The Lorentzian half width at half maximum (HWHM) is $\Delta\nu_{\mathrm{L}} = \Gamma/2 + \gamma_{\mathrm{c}}$, where $\Gamma$ is the natural width and $\gamma_{\mathrm{c}}$ is the collisional broadening width. Because the latter is considered to be very small, $\gamma_{\mathrm{c}}$ can be ignored. We considered $\Delta\nu_{\mathrm{L}}$ to be $1.2 \times 10^{-4}$ $\mathrm{cm}^{-1}$, as calculated from the lifetime of $4P'[3/2]$. The Gaussian HWHM $\Delta\nu_{\mathrm{D}}$ and $S$ were determined using least-squares fitting, where $\Delta\nu_{\mathrm{L}}$ was fixed to the value given above to eliminate correlation with $S$. The sweep axis agreed with those obtained within experimental uncertainty.

First, we calculated the gas temperature from the Doppler width using the relationship $\delta\nu_{\mathrm{D}} = 7.16 \times 10^{-7} \nu_0 (T/M)^{1/2}$ given in Ref. [7]. The results are shown in Fig. 3. The experimental conditions were as follows: operational discharge currents, 1–400 mA; gas pressure, 1.3–6.7 Pa. The gas temperature increases linearly from 297 to 460 K with increasing discharge current. The temperature $T(P, I)$ can be described by the first-order equa-

tion

$$T(P, I) = a_{00} + a_{10}P + a_{01}I + a_{11}PI. \quad (3)$$

TABLE

Parameters determined by least-squares fitting.

| Parameters for Eq. 3 | | | st. dev. 3.2 K |
|---|---|---|---|
| $a_{00}$ [K] | 294.0(16) | $a_{01}$ [K/mA] | 0.2706(92) |
| $a_{10}$ [K/Pa] | 2.93(33) | $a_{11}$ [K/Pa mA] | 0.0141(21) |
| Parameters for Eq. 5 [$\times 10^8$ cm$^{-3}$] | | | st. dev. 0.47 |
| $A_{00}$ | 13.06(22) | $A_{11}$[mA$^{-1}$ Pa$^{-1}$] | 0.0189(13) |
| $A_{10}$[Pa$^{-1}$] | −1.156(46) | $A_{21}$[Pa$^{-2}$ mA$^{-1}$] | $2.64(148) \times 10^{-4}$ |
| $A_{01}$[mA$^{-1}$] | −0.0022(21) | $A_{12}$[Pa$^{-1}$ mA$^{-2}$] | $-1.05(14) \times 10^{-5}$ |

The parameters for Eq. (3) are listed in the Table. $a_{00}$ is the gas temperature at zero current taken to be the reference temperature $T_0 = 294$ K.

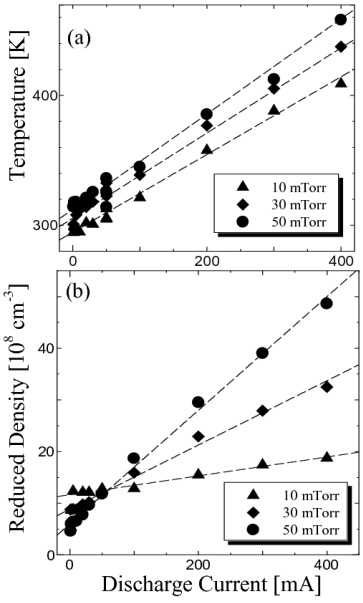


Fig. 3. Experimental results. (a) Thermodynamic temperature $T$ as a function of discharge current and calculated line (dashed lines) from Eq. (3). (b) Reduced atomic density of the $4S'[1/2]0$ state as a function of discharge current. The dash lines are the fit to the observed values using the parameters of the Table.

Next, we calculated the population density $N(P, I)$ of the $4S'[1/2]0$ state from line intensity $S$ using the relation [8]

$$S(T) = \frac{\mathrm{e}^2}{4\varepsilon_0 m_\mathrm{e} c^2} \cdot N_{4S'} \cdot f_{4S'\to 4P'} \cdot L, \quad (4)$$

where $L$ is the cell length and $f$ is the oscillator strength [6]. We reduced the atomic density $N_{4S'[1/2]0}(T)$ to the reference temperature by multiplying it by the factor $(T/294)$, where $T$ is the temperature shown in Fig. 3a. The change in reduced population density $N(T_0,\ P,\ I)$ with current is shown in Fig. 3b. The slope $\delta N/\delta I \propto P$ and the intercept are constant. $N(T_0, P, I)$ can be expressed by the polynomial

$$N(T_0, P, I) = \sum_{i,j=0} P^i I^j. \quad (5)$$

We used least-squares fitting to determine the parameters $A_{ij}$. The results for the first six parameters are listed in the Table. By joint analysis with Eq. (3), we obtained a simple relation for population density at discharge current $I$ and gas pressure $P$

$$N(P, I) \cong N(T_0, P, I) \cdot \frac{T_0}{T(P, I)}, \quad (6)$$

where the error in constant $a_{00}$ can be determined from the estimation of collisional width and results in an error for $A_{00}$, while the other constants are based on $I(ref, \nu)$, $I(100\%, \nu)$ and the linearity of the frequency sweep.

## 4. Conclusion

We demonstrated the utility of high-resolution laser spectroscopy for determining FTS sputter gas temperature and density. Disturbance from the static magnetic field is eliminated by choosing the transition $\Delta M_J = 0$ and $J = 0 \leftrightarrow 1$. The thermodynamic temperature of the $4S'[1/2]0$ state is determined from the Doppler width at a discharge current in the range 1–400 mA and a gas pressure in the range 1.3–6.6 Pa. Obtained population densities are reduced to the reference temperature, which is related to discharge current and gas pressure by an empirical equation.

## References

[1] T. Uchida, S. Kaneta, M. Ichihara, M. Ohtsuka, T. Otomo, D. Marx, *Jpn. J. Appl. Phys.* **44**, 282 (2005).

[2] Y. Hoshi, H. Kato, K. Funatsu, *Thin Solid Films* **445**, 245 (2003).

[3] R. Ohki, T. Hoshi, *Trans. IEICE, J.83-C* **8**, 715 (2000) (in Japanese).

[4] M.F. Dony, J.P. Dauchot, M. Wautelet, M. Hecq, A. Ricard, *J. Vac. Sci. Technol. A* **18**, 809 (2000).

[5] N. Britun, M. Gaillard, Y.M. Kim, K.S. Kim, J.G. Han, *Met. Mater.–Ins.* **13**, 483 (2007).

[6] Y. Ralchenko, A.E. Kramida, J. Reader, and NIST ASD Team (2008). NIST Atomic Spectra Database (version 3.1.5) [online].

[7] W. Demtröder, *Laser Spectroscopy Basic Concepts and Instrumentation*, 3rd ed., Springer 2002.

[8] A. Mitchell, M. Zemansky, *Resonance Radiation and Excited Atoms*, Cambridge 1971.